Failure Analysis of a Conveyor Belt Rail (Tripper) of Mineral

Carlos Fosca(✉)

Pontificia Universidad Católica del Perú, Lima, Peru
cfosca@pucp.edu.pe

Abstract. A failure analysis of a fractured rail corresponding to a railway conveyor belt (Tripper) that operated in service for two years has been carried out. A visual inspection, chemical composition analysis, metallographic analysis, hardness and microhardness measurements were carried out on the failed piece. The rail was made of 0.89% C carbon steel and presented a decarburized area on the running surface, with strong plastic deformation due to the operation and work hardened. The metallurgical root cause is associated with the presence of proeutectoid ferrite and non-metallic inclusions that have been severely deformed by rolling stresses, generating a weak continuous region that nucleated rolling contact fatigue cracks (RCF) and accelerated the formation of a longitudinal crack that propagated vertically (vertical split head) as a consequence of other possible material defects.

Keywords: rolling contact fatigue · rail fracture · rail failure analysis

1 Introduction

One of the most common failures in the rails is the fracture due to rolling contact fatigue (Rolling Contact Fatigue), this failure mechanism can have multiple manifestations in the rail as “Gauge Corner Checking”, “Head checking”, “ Pitting”, “Spalling”, etc. [1]. However, it is also possible that manufacturing defects may occur that cause breaks in service, as is the case with the vertical cracking of the rail head (vertical split head) [2]. Another important factor in fatigue life of a rail is the degree of cold deformation hardening that has experienced the rolling area. As a result, there is a materials anisotropy, that strongly affects the development of rolling contact fatigue (RCF) [3].

The present study corresponds to the fractured rail failure analysis corresponding to a mineral conveyor belt (tripper). Figure 1 shows a piece of the fractured rail next to an unused rail, which were supplied to determine the root cause of the failure. The tripper has four wheels per side, the rails support vertical forces of up to 1027 KN. The amount of cycles per day is 250 on average. After two years of operation, the rail system suffers the fracture at one of its ends.

According to the information provided, the steel of the rail corresponds to a CR104 Steel Head Hardened (HH) and fits the ASTM A759-10 specifications.

A. Vizán Idoipe and J. C. García Prada (Eds.): IACME 2022, *Proceedings of the XV Ibero-American Congress of Mechanical Engineering*, pp. 64–69, 2023.
https://doi.org/10.1007/978-3-031-38563-6_10

Fig. 1. View of the parts of a rail system, supplied for analysis.

2 Results and Analysis

To carry out this fault analysis, the following tests and analysis were carried out:

- Visual and magnetic particles
- Chemical analysis of the rail material
- Hardness tests.
- Metallographic and micro-hardness measurements

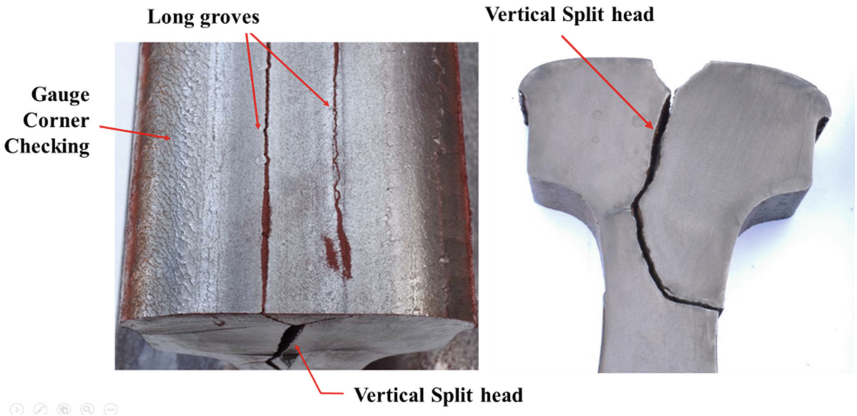

Fig. 2. Long grooves, gauge corner checking and vertical split heads present in the fractured rail.

2.1 Visual Inspection

Two longitudinal cracks (long grooves) were observed on the head of the rail (Fig. 2) that spread into the interior of the material. Subsequently, a vertical crack was developed (vertical split Head). Another important observation is the strong plastic deformation observed in the head of the rail, appreciating a reduction in the height of the same of 3 mm and a widening of the edge of the rail (gauge corner region).

2.2 Chemical Composition Analysis

Samples of the fractured rail and the new rail for their corresponding chemical analysis were extracted. The analysis was performed by optical emission spectrometry according with the ASTM E60-11 standard, the analysis result is shown in Table 1.

Table 1. Chemical composition (% weight) of the failed rail and the new rail

sample	C	Mn	Si	P	S	Ni	Cr	Mo	Cu	V
New Rail	0.80	0.93	0.35	0.014	0.010	0.13	0.19	0.04	0.31	0.00
Cracked rail	0.89	0.68	0.38	0.009	0.009	0.12	0.26	0.03	0.28	0.10
ASTM A759-10	0.67 - 0.84	0.70 – 1.10	0.10 – 0.50	0.04 Max.	0.05 Max.	----	----	----	-----	----

From the chemical analysis results, it can be concluded that the materials of both rail sections comply with the material specifications for crane rails according to the ASTM standard to 759-10. However, the fractured rail presents a slightly higher C content (0.89%C).

2.3 Hardness Measurement

Transversal sections of the supplied rails (new and fractured) were cut. Hardness measurements were carried out using a Equotip® Leeb hardness portable equipment. The new rail presented a hardness in its cross section that ranged between 292–366 HB while the fractured rail had a hardness between 336 and 393 HB. According to ASTM A759-10, high strength rails must have a HB hardness between the range of 321 to 388. According to this, the hardness of the fractured rail conforms better to the specification's standard.

2.4 Metallographic Analysis

A metallographic analysis was carried out in samples extracted from the portion of the new rail and the fractured rail. The metallographic etching was performed using 2% Nital

reagent. The microstructure of the new rail in the surface of the head was Proeutectoid Ferrite (F) and Perlite (P) (Fig. 3.a) while the microstructure of the area immediately under the surface was constituted by equiaxial grains of Perlite (P) (Fig. 3.b). This last microstructure is close correlation with the chemical composition of the steel of the analyzed rail. The microstructure of the head surface is consequence of a decarburization process during the rail manufacturing.

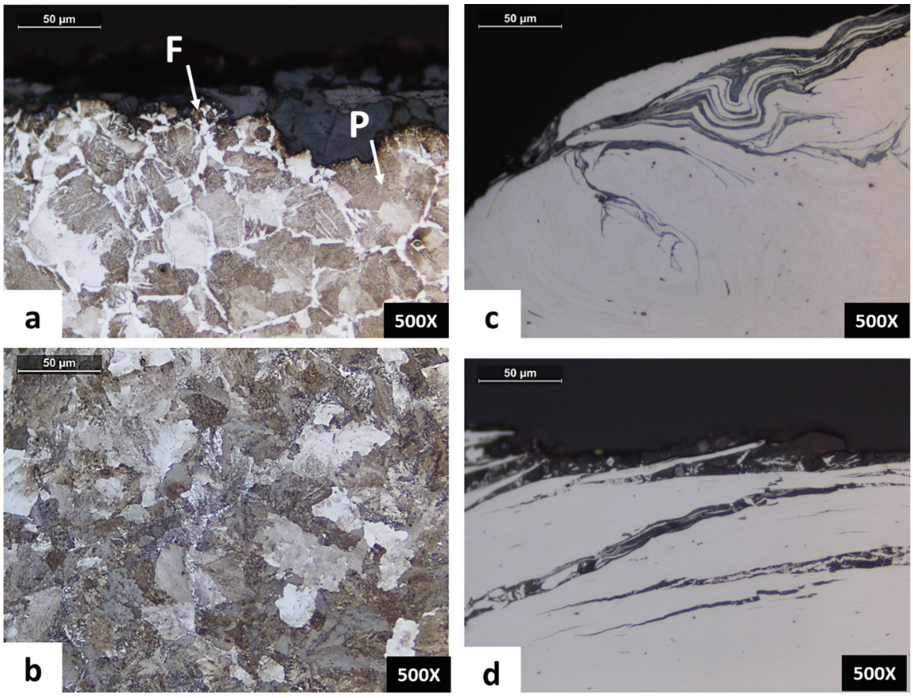

Fig. 3. [a] [b] Micrographs of the original rail (new) showing decarburation zone in the surface [a] (etching: 2% Nital). [c][d] Non etching micrographs of the head zone of failed rail showing non-metallic inclusions strongly deformed and aligned [c] and propagation of micro-cracks following the paths of aligned non-metallic inclusions [d].

The head of the fractured rail presented in the rolling contact area a strong plastic deformation (180–350 microns) that caused the deformation and realignment of non -metallic inclusions (Fig. 3.c). In addition, microcracks that follow the paths of the realigned non-metallic inclusions were observed (Fig. 3.d).

2.5 Micro Hardness Measurement

The strain-hardening layer observed in the head of the fractured rail presented hardness values of up to 573 HV0.5, while the region of the material away from the hardened area it presented hardness between 412–430 HV0.5 (See Fig. 4). Due to the differences in mechanical properties between the pro-eutectoid ferrite (decarburized zones), much

more ductile, and the perlite, the deformation does not occur uniformly at the microstructural level and the pro-eutectoid ferrite is constituted in points of preferential start of fatigue micro-cracks [4–6]. Similarly, ductile non-metallic inclusions such as manganese sulfide can become nucleation points of rolling contact fatigue cracks (RCF) in strongly deformed areas of the rolling surface [7].

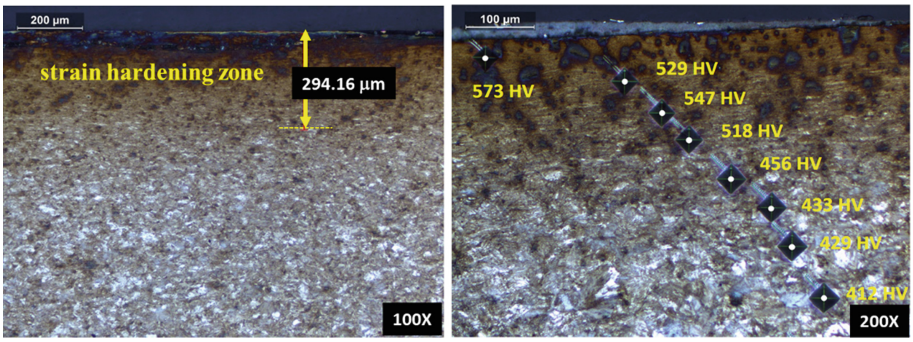

Fig. 4. Micrographs of samples extracted from the head of the fractured rail where the strain-hardening zone and the hardness (HV0.5) values can be seen

These surface cracks are caused by the contact stresses between the crane wheel and the rail. The mechanism that originates them is known as rolling contact fatigue (RCF). These cracks grow preferably in the riel longitudinal direction, but they also spread in the other directions due to the triaxial load system that occurs inside the rail due to the load with the wheel [8]. The trajectory of the crack is determined by the load, the anisotropy of the plastically deformed layer and the weaknesses of the material [3].

The nucleation of these longitudinal surface cracks can have its origin in numerous causes, such as hardening by high localized plastic deformation, presence of non-metallic inclusions aligned (oxides, sulphides) that act as stresses micro-concentrators, surface defects such as laminations, etc.

3 Conclusions

The fractured rail exhibited a combination of defects that acted synergistically in its premature failure (approximately two years). The head rail presented a decarburized surface with the presence of pro-eutectoid ferrite, which coupled with the presence of segregation of realigned non-metallic inclusions, caused a mechanically weak region, compared to the severely strain hardened pearlite.

The cyclic loading originated by the contact between the wheel and the rail, generated rolling contact fatigue damage in different parts of the head of the rail (gauge corner checking) and long grooves more associated with laminations or manufacturing defects, but that was accelerated by cracking in strain hardened layer due to contact fatigue. The confluence of these cracking fronts resulted in the fracture of the component through a vertical crack (vertical Split Head).

References

1. Office of Railroad Safety: Track Inspector Rail Defect Reference Manual. Federal Railroad Administration, USA (2015)
2. NSW: Rail Defects Handbook. Engineering Manual Track, RailCorp Network (2012)
3. Schilke, M.: Degradation of Railway Rails from a Materials Point of View. Chalmers University of Technology, Göteborg, Sweden (2013)
4. Chard, A.: Deformation of Inclusions in Rail Steel Due to Rolling Contact. University of Birmingham, Birmingham (2011)
5. Beynon, J.H., Garnham, J.E., Sawley, K.J.: Rolling contact fatigue of three pearlitic rail steels. Wear **192**, 94–111 (1996)
6. Davis, C.L., Garnham, J.E.: The role of deformed rail microstructure on rolling contact fatigue initiation. Wear **265**, 1363–1372 (2008)
7. Garnham, J.E., Ding, R.-G., Davis, C.L.: Ductile inclusions in rail, subject to compressive rolling–sliding contact. Wear **269**, 733–746 (2010)
8. Németh, A.: Case Studies in Railway Construction: Rolling Contact Fatigue Rail Defects. Széchenyi István University, Győr, Hungary (2017)